Force evaluations in lattice Boltzmann simulations with moving boundaries in two dimensions

Huabing Li,[1,2,3] Xiaoyan Lu,[2] Haiping Fang,[1,4,*] and Yuehong Qian[5]
[1]*Shanghai Institute of Applied Physics, Chinese Academy of Sciences, P.O. Box 800-204, Shanghai 201800, China*
[2]*Surface Laboratory and Department of Physics, Fudan University, Shanghai 200433, China*
[3]*Department of Computational Science and Applied Physics, Guilin University of Electronic Technology, Guilin 541004, China*
[4]*Department of Physics, Zhejiang Normal University, Jinhua 321004, China*
[5]*Department of Mechanical and Aerospace Engineering, Princeton University, New Jersey 08544, USA*
(Received 3 March 2004; published 9 August 2004)

Two techniques, based on the exchange of momentum and the integration of stress tensor, for the evaluation of the hydrodynamic forces in the lattice Boltzmann simulations are investigated on the curved and moving boundaries in two dimensions. The following results are obtained by numerical simulations: (i) the hydrodynamic forces on an inclined boundary and arc in liquid without flow computed by the stress-integration method agree with analytical predictions to a very high accuracy, while those by the momentum-exchange method have considerable errors for small segments; (ii) the simulation results of the sedimentation of a circular cylinder in a two-dimensional channel with the stress-integration method for hydrodynamic forces are in excellent agreement with those by a second-order moving finite-element method; (iii) the particle migrated from the centerline is found to occur in the simulations of a circular cylinder in a Poiseuille flow by the stress-integration method, consistent with the Segré-Silberberg effect. In conclusion, the stress-integration method can be a good candidate to evaluate the hydrodynamic forces on the elastic boundaries and moving particles in fluid.

DOI: 10.1103/PhysRevE.70.026701 PACS number(s): 47.11.+j, 83.85.Pt, 47.10.+g, 82.70.Kj

I. INTRODUCTION

Since the pioneering work by Ladd [1], the lattice Boltzmann method [2–5] has been a popular tool to simulate solid particle moving in fluids. The ingredients of such a lattice Boltzmann simulation usually include: lattice Boltzmann simulations in the fluid domain, nonslip boundary conditions at solid-liquid boundaries, appropriate hydrodynamic force on the solid, and a second-order Newtonian dynamics to update the position, rotation, velocity, and angular velocity of particles. Ladd extended the bounce-back rule for moving particles and developed a formula to calculate the hydrodynamic force exerting on the solid particles based on the momentum exchange [1,6,7]. Aidum *et al.* [8,9] attempted to improve Ladd's model by removing the fluid within the solid region so that they could handle a system with solid density less than fluid density and conserved the fluid mass exactly. Qi [10] applied the model to simulate the nonspherical particles in nonzero Reynolds number flow. Behrend [11] analyzed different boundary conditions based on the bounce-back rule and proposed a "related bounce back at the nodes" (RBBN). Recently Raiskinmak *et al.* [12] applied the Behrend method to simulate nonspherical particles suspended in a shear flow. Migliorini *et al.* [13] used a lattice Boltzmann approach to quantify the forces exerted on rolling leukocytes by red blood cells in "virtual blood vessels." Almost all previous lattice Boltzmann methods for suspension particles have assumed the physical boundary is located at the middle of the mesh link between a solid node and a fluid node. The hydrodynamic radius of a suspended particle differs from the input radius [12].

The determination of the hydrodynamic force involving curved and moving boundaries is an important issue in the application of the lattice Boltzmann method to the simulations of the particle suspensions. All the above simulations evaluate the hydrodynamic force by the momentum-exchange method [1,11]. The momentum-exchange method is easy to be implemented and the accuracy to calculate the hydrodynamic force exerting on the rest solid particles has been demonstrated [14–17].

On the other hand, He and Doolen [18] calculated the force by integrating the total stress on the surface on the cylinder and the components of the stress tensor were obtained by taking respective velocity gradients. In the method of integrating stress tensor, the stress tensor is derived from further processing of the distribution functions, such as extrapolation. Recently, Mei *et al.* compared the simulation results of several test cases with fixed and complex boundaries and found that the momentum exchange is superior to the stress integration [14].

In this paper we will examine the technique of stress integration for force evaluation in the lattice Boltzmann simulation on curved and moving boundaries in two dimensions by using the formula proposed by Inamuro *et al.* [19] to calculate the stress tensor. Excellent agreement is obtained on the particle motions at small Reynolds numbers, including the particle velocity, the particle angular velocity, and the forces and torques on the moving particles by numerical simulating of the sedimentation of a circular cylinder in a two-dimensional channel and comparing with those from a finite-element method [20–22]. Moreover, the simulation on neutrally buoyant cylinders in a horizontal pipe flow with this method shows that the particles migrate laterally away both from the wall and the centerline and reach a certain lateral equilibrium position that is consistent with the Segré-Silberberg effect [23] observed in 1961. It is worth com-

*Author to whom correspondence should be addressed. Email address: hpfang2000@yahoo.com

menting here that the equation to calculate the stress tensor derived by Inamuro *et al.* [19], which avoids velocity gradients, is applied in the lattice Boltzmann simulations so that not only the noise in the simulations is efficiently reduced, but also the code is simpler.

The paper is organized as follows. In Sec. II we briefly describe the lattice Boltzmann method. Section III and IV review the boundary condition and the two methods to evaluate hydrodynamic forces exerted on the complex and moving boundary. The numerical simulation results are shown in Sec. V. In Sec. VI, the conclusion and discussion are presented.

II. THE LATTICE BOLTZMANN MODEL

The Boltzmann equation with the single relaxation time approximation reads [24]

$$\frac{\partial f}{\partial t} + \boldsymbol{\zeta} \cdot \boldsymbol{\nabla} f = -\frac{1}{\lambda}[f - f^{(eq)}], \tag{1}$$

where ζ is the particle velocity, $f^{(eq)}$ is the equilibrium distribution function, and λ is the relaxation time.

Discretizing Eq. (1) in the velocity space ζ by using a finite set of velocities $\mathbf{e}_i$, we obtain [25,26]

$$\frac{\partial f_i}{\partial t} + \mathbf{e}_i \cdot \boldsymbol{\nabla} f_i = -\frac{1}{\lambda}[f_i - f_i^{(eq)}]. \tag{2}$$

In the model on a square lattice in two dimensions, $\mathbf{e}_0 = (0,0)$, $\mathbf{e}_i = c[\cos \pi(i-1)/2, \sin \pi(i-1)/2]$, $i=1,2,3,4$, and $\mathbf{e}_i = c[\cos \pi(2i-1)/4, \sin \pi(2i-1)/4]$, for $i=5,6,7,8$ are the nine possible velocity vectors (D2Q9), and the equilibrium distribution functions are of the form [3,25]

$$f_i^{eq} = \alpha_i \rho \left[1 + \frac{3}{c^2}\mathbf{e}_i \cdot \mathbf{u} + \frac{9}{2c^4}(\mathbf{e}_i \cdot \mathbf{u})^2 - \frac{3}{2c^2}u^2 \right], \tag{3}$$

for athermal fluids. In the equation, $\alpha_0 = 4/9$, $\alpha_1 = \alpha_2 = \alpha_3 = \alpha_4 = 1/9$, and $\alpha_5 = \alpha_6 = \alpha_7 = \alpha_8 = 1/36$, $c = \delta x/\delta t$ is the lattice speed, and δx and δt are the lattice constant and the time step, respectively. The density ρ and the velocity $\mathbf{u}$ are defined by

$$\rho = \sum_i f_i,$$

$$\mathbf{u} = \sum_i f_i \mathbf{e}_i / \rho. \tag{4}$$

The lattice Boltzmann equation [4,3,5] is obtained by further discretizing Eq. (2) in space $\mathbf{x}$ and time t as

$$f_i(\mathbf{x} + \delta x \mathbf{e}_i, t + \delta t) - f_i(\mathbf{x}, t) = -\frac{1}{\tau}(f_i - f_i^{eq}), \tag{5}$$

where $\tau = \lambda/\delta t$. The macroscopic equations can be obtained by a Chapman-Enskog procedure. The viscosity in the macroscopic equations is

$$\nu = \frac{(2\tau - 1)}{6} c^2 \delta t. \tag{6}$$

In this paper, we set $\delta x = \delta t = c = 1$.

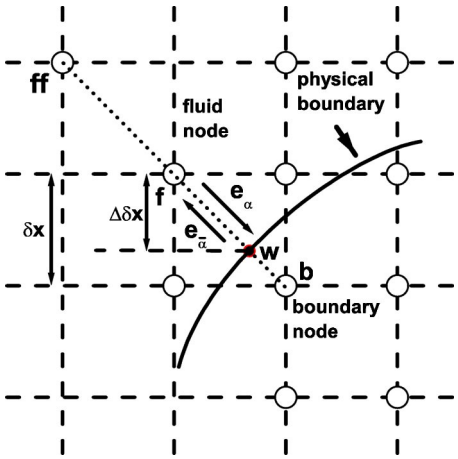

FIG. 1. The layout of the regularly spaced lattices and curved wall boundary.

III. BOUNDARY CONDITION FOR COMPLEX GEOMETRY

Filippova and Hanel [27] presented their scheme for the treating of a boundary condition by considering a curved boundary lying between the lattice node of space $\Delta\delta x$ as shown in Fig. 1. The lattice nodes on the solid and fluid side are denoted by $\mathbf{x}_b$ and $\mathbf{x}_f$, respectively. We assume

$$\mathbf{e}_i = \mathbf{x}_b - \mathbf{x}_f$$

and

$$\mathbf{e}_{\bar{i}} = -\mathbf{e}_i.$$

The filled small circle at $\mathbf{x}_w$ marked by a letter w, is the intersection with the the physical boundary on the link between $\mathbf{x}_b$ and $\mathbf{x}_f$. The fraction of an intersected link in the fluid is Δ.

$$\Delta = \frac{|\mathbf{x}_f - \mathbf{x}_w|}{|\mathbf{x}_f - \mathbf{x}_b|}, \quad 0 \leqslant \Delta \leqslant 1. \tag{7}$$

After the collision step, at time t, the distribution functions at $\mathbf{x}_f$ are known. In the streaming step, $f_{\bar{i}}(\mathbf{x}_f)$ is expected to obtained by

$$f_{\bar{i}}(\mathbf{x}_f, t + \delta t) = f_{\bar{i}}(\mathbf{x}_b, t). \tag{8}$$

However, the distribution function $f_{\bar{i}}(\mathbf{x}_b, t)$ at the boundary node b is unknown.

Filipova and Hanel assumed the linear interpolation [27]

$$f_{\bar{i}}(\mathbf{x}_b, t) = (1 - \chi) f_i(\mathbf{x}_f, t) + \chi f_i^{(*)}(\mathbf{x}_b, t) + 6\alpha_i \mathbf{e}_{\bar{i}} \cdot \mathbf{u}_w, \tag{9}$$

where $\mathbf{u}_w = \mathbf{u}(\mathbf{x}_w, t)$ is the velocity at $\mathbf{x}_w$ and χ is a parameter. $f_i^{(*)}$ is a fictitious equilibrium distribution function given by

$$f_i^{(*)}(\mathbf{x}_b, t) = \alpha_i \rho \left[1 + 3\mathbf{e}_i \cdot \mathbf{u}_{bf} + \frac{9}{2}(\mathbf{e}_i \cdot \mathbf{u}_f)^2 - \frac{3}{2}u_f^2 \right], \tag{10}$$

where $\mathbf{u}_f = \mathbf{u}(\mathbf{x}_f, t)$ is the fluid velocity at the fluid node f shown in Fig. 1, $\mathbf{u}_{bf}$ is to be determined below. Filipova and Hanel proposed [27]

$$\mathbf{u}_{bf} = (\Delta - 1)\mathbf{u}_f/\Delta + \mathbf{u}_w/\Delta \text{ and } \chi = (2\Delta - 1)/\tau$$

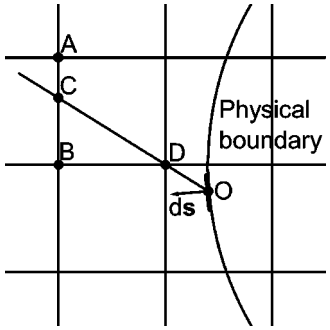

FIG. 2. A schematic diagram of extrapolation. The distribution functions at point *C* is obtained by linear interpolation from nodes *A* and *B*. The distribution functions at point *O* on the boundary of the cylinder is computed by linear extrapolation from *C* and *D*.

$$\text{for } \Delta \geqslant \frac{1}{2}, \tag{11}$$

and

$$\mathbf{u}_{bf} = \mathbf{u}_f \text{ and } \chi = (2\Delta - 1)/(\tau - 1) \text{ for } \Delta \leqslant \frac{1}{2}, \tag{12}$$

to obtain a second-order scheme for the "slow flow." Mei *et al.* [28] improved the stability of the scheme by replacing Eq. (12) with

$$\mathbf{u}_{bf} = \mathbf{u}_{ff} \text{ and } \chi = (2\Delta - 1)/(\tau - 1) \text{ for } \Delta \leqslant \frac{1}{2}, \tag{13}$$

where $\mathbf{u}_{ff}$ is the fluid velocity at fluid node *ff* shown in Fig. 1. They have used the improved technique to test against several flow problems, such as the two-dimensional channel flows with constant and oscillating pressure gradients, flow due to impulsively started wall, lid-driven square cavity flow, and flow over a column of circular cylinders to demonstrate its accuracy and robustness [28]. This boundary treatment will be adopted in the present paper.

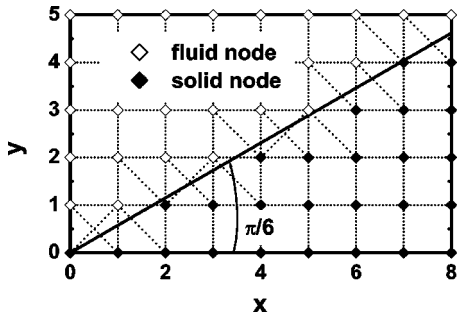

FIG. 3. A schematic diagram of an inclined boundary in lattice Boltzmann simulations. The heavy line is the boundary. The dotted lines are the links connecting fluid nodes and solid nodes.

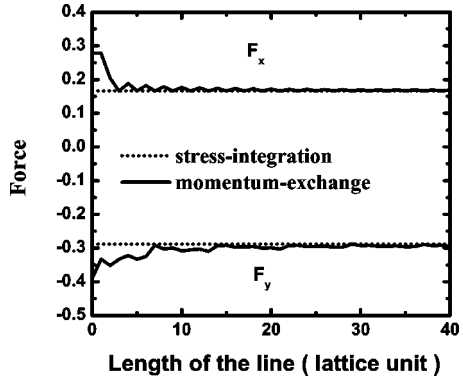

FIG. 4. The hydrodynamic force per unit length of the boundary in *x* and *y* directions, respectively. The dotted lines are the results from the stress-integration method which are consistent with analytical predictions exactly. The solid lines are calculated from the method of momentum exchange and averaged from 0 to *x*.

IV. METHODS FOR FORCE EVALUATION IN THE LATTICE BOLTZMANN METHOD

A. Method based on momentum exchange

For each *relevant* direction $\mathbf{e}_i$ from a fluid node to a boundary node, the solid boundary obtained an amount of momentum $f_i(\mathbf{x}_b,t)\mathbf{e}_i - f_i(\mathbf{x}_f,t_+)\mathbf{e}_{\bar{i}}$, where the first term is due to a fraction of particles $f_i(\mathbf{x}_f,t_+)$ colliding on the boundary and the second term comes from a fraction of particles $f_{\bar{i}}(\mathbf{x}_b,t)$ bouncing back from the boundary in a time step. Consequently, the hydrodynamic force exerted on the solid particle at time *t* along this direction is

$$\mathbf{F}(\mathbf{x}_b) = [f_{\bar{\alpha}}(\mathbf{x}_b,t) + f_\alpha(\mathbf{x}_f,t_+)]\mathbf{e}_\alpha, \tag{14}$$

where t_+ is the post collision time, and $f_{\bar{\alpha}}(\mathbf{x}_b,t)$ is obtained from Eq. (9). The particle force $\mathbf{F}_T$ and torque $\mathbf{T}_T$ acting on the solid particle are obtained as

$$\mathbf{F}_T = \sum \mathbf{F}(\mathbf{x}_b) \tag{15}$$

and

$$\mathbf{T}_T = \sum (\mathbf{x}_b - \mathbf{R}) \times \mathbf{F}(\mathbf{x}_b), \tag{16}$$

where $\mathbf{R}$ is the center of mass of the solid particle. The summation runs over all the relevant directions of the boundary node.

B. Force evaluation based on stress integration

According to those proposed by Inamuro *et al.*, the stress tensor in the lattice Boltzmann method can be calculated as follows [19]:

$$\sigma_{ij} = -\frac{1}{6\tau}\rho\delta_{ij} - \left(1 - \frac{1}{2\tau}\right)\sum (e_{\alpha i} - u_i)(e_{\alpha j} - u_j)f_\alpha, \tag{17}$$

where δ_{ij} is the Kronecker delta function and $i,j = x,y$. This process avoids using velocity gradients to calculate the stress tensor. Denoted by *S* the surface of the cylinder, the hydro-

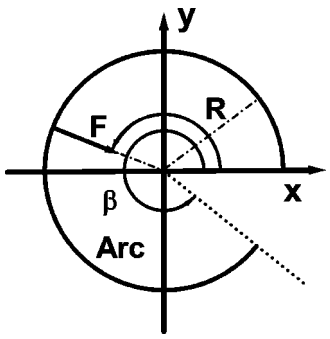

FIG. 5. An arc of radian β and radius R in fluid.

dynamic force and torque are calculated by integrating stress tensor and momentum flux on S [19]

$$\mathbf{F} = \int_S \{\sigma \cdot \mathbf{n} - \rho \mathbf{u}[(\mathbf{u} - \mathbf{V}) \cdot \mathbf{n}]\} \cdot \mathrm{ds},$$

$$\mathbf{T} = \int_S \mathbf{r} \times \{\sigma \cdot \mathbf{n} - \rho \mathbf{u}[(\mathbf{u} - \mathbf{V}) \cdot \mathbf{n}]\} \cdot \mathrm{ds}, \qquad (18)$$

where $\mathbf{n}$ is the unit outward normal vector on S, $\mathbf{r}$ is a vector from the center of the cylinder to the point on S, $\mathbf{V}$ is the velocity of the center of mass of the solid particle. The integral in Eqs. (18) is approximated by the numerical quadrature of 400 points.

In the calculation of σ_{ij} on S, f_α on S is obtained from extrapolation as follows, while $\mathbf{u}$ on S can be computed from f_α. Figure 2 shows an example of extrapolation. The distribution function at C is obtained by linear interpolation from those at the nodes A and B. The distribution functions at O are computed by linear extrapolation from those at the points C and D. The final distribution functions at the point O for the calculation of σ_{ij} is the average of the extrapolated values of all the *relevant* directions. A relevant direction is defined here as a direction from O to a nearest-neighbored or next nearest-neighbored fluid node (D, for example). In order to increase the stability of the scheme, we establish the following restrictions on the choice of the *relevant* directions: (A) The angle between the relevant direction and the normal direction $\mathbf{n}$ of the boundary is smaller than 90°; (B) $\Delta = CD/CO \geqslant 0.5$.

The method based on momentum exchange does not reduce the stability of the lattice Boltzmann simulations. The extrapolation, on the other hand, usually causes instability. We have performed many numerical simulations based on the stress integration and found that it is stable for low-particle Reynolds numbers (which will be defined in Sec. IV C), i.e., $\mathrm{Re} < 10$, when τ is in the range $0.51 < \tau < 0.98$ in all the numerical simulations of the tested problems in the present paper. In the special case that there is not any relevant direction for extrapolation available, we suggest that the distribution functions at O are those at the nearest-neighbored fluid node of O and the accuracy of this suggestion should be tested and presented elsewhere.

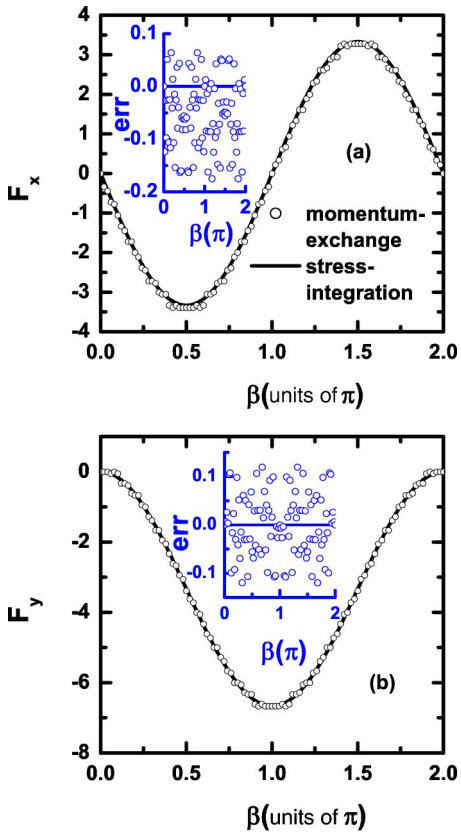

FIG. 6. The hydrodynamic force $\mathbf{F}$ from outside on the arc is shown in Fig. 5 in x and y directions. The solid lines and the symbols are the numerical results from the methods based on stress integration and momentum exchange, respectively. The insets in (a) and (b) show the errors.

V. SIMULATION RESULTS AND DISCUSSION

A. Hydrodynamic force on an inclined boundary

When the lattice Boltzmann method is applied to simulate the flow in a tube with elastic boundaries such as the artery [29–31], the hydrodynamic force on a curved boundary will have to be evaluated. Moreover, since the motion of each boundary segment depends on the forces acting on it, the accurate calculation of the hydrodynamic force on each small segment is of crucial importance. In this subsection, the dependence of the errors on the length of the boundary segments is investigated in the system shown in Fig. 3. For simplicity, we assume that there is no fluid flow in the system and pressure in fluid keeps as a constant p. In lattice Boltzmann simulations, equilibrium distribution functions with zero velocity and a fixed density $\rho = 3p$ are set on all the fluid nodes, i.e., $f_\alpha = f_\alpha^{eq}$. Stress tensor can obtained from Eq. (17) as

$$\sigma_{ij} = -\frac{1}{3}\rho \delta_{ij}, \qquad (19)$$

and the hydrodynamic force acting on a segment of the boundary with a length dl is:

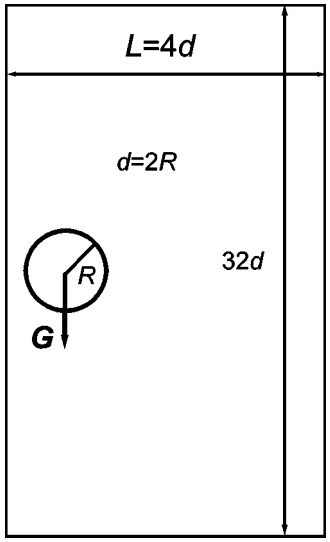

FIG. 7. A schematic diagram of a circular particle in a two-dimensional vertical channel ($L=4d$) released near one wall. **G** is the gravity.

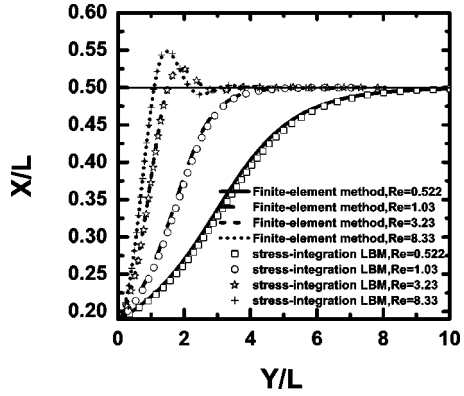

FIG. 8. Settling trajectory for circular cylinders released at $x=0.076$ cm at small Reynolds numbers *Re*. The lines are the numerical results from a second-order moving finite-element method [21]. The symbols are the simulation results from the present lattice Boltzmann scheme with stress-integration method.

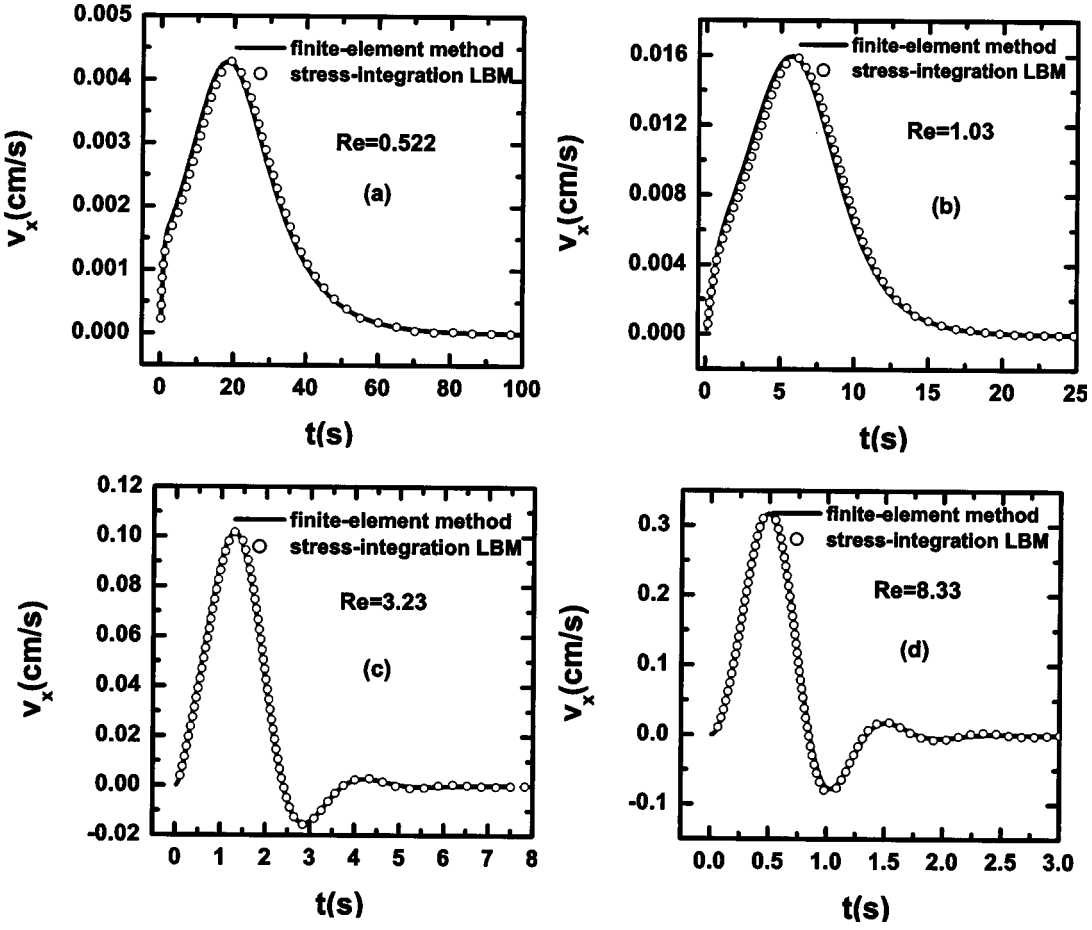

FIG. 9. The time-dependent particle velocity in horizontal directions at different Reynolds numbers.

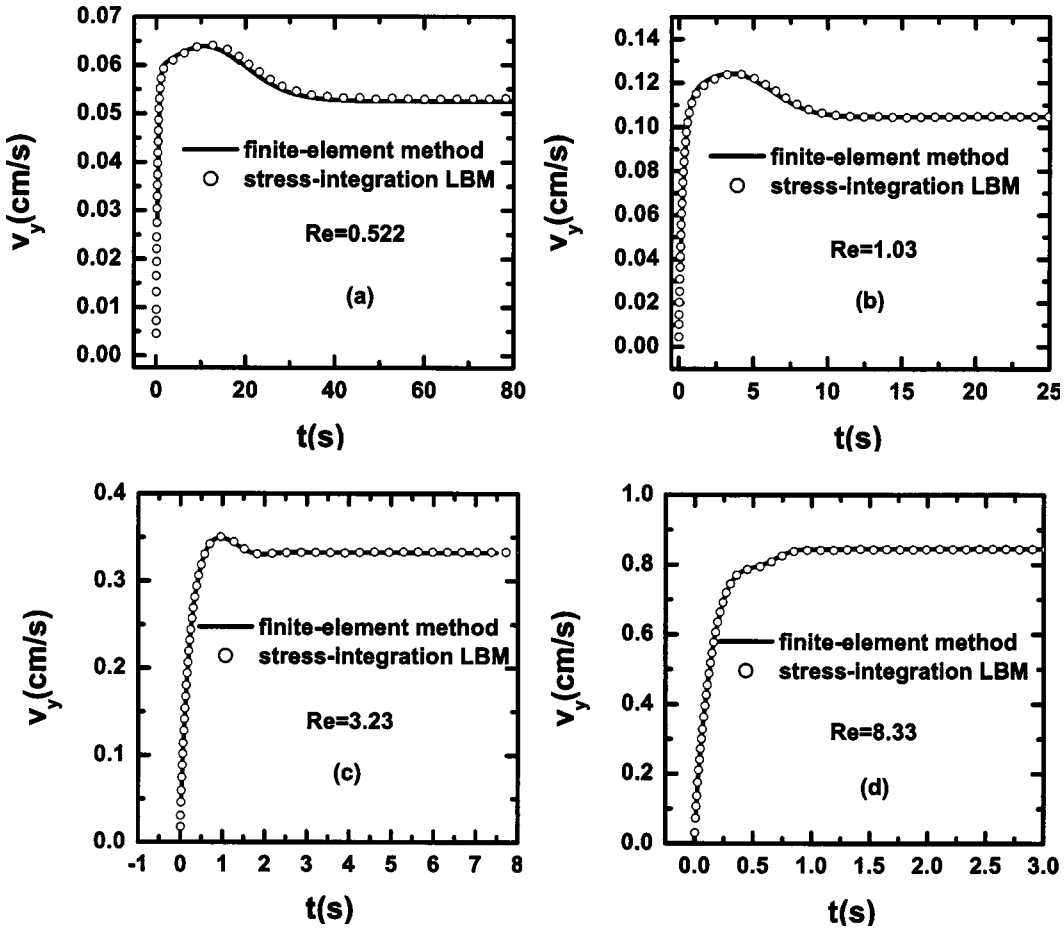

FIG. 10. The time-dependent particle velocity in vertical directions at different Reynolds numbers.

$$d\mathbf{F} = \frac{1}{3}\rho dl\,\mathbf{n}, \tag{20}$$

where **n** is the unit vector perpendicular to the boundary. This is exactly the analytical result.

Figure 4 displays the hydrodynamic force per unit length of the boundary calculated from the method of momentum exchange and averaged from 0 to x. It is clear that there are large errors for small x, i.e., the method of momentum exchange gives large errors for small segments and is not suitable for the simulations of the systems with elastic boundaries.

B. Hydrodynamic force on arcs

The arc shown in Fig. 5 gives another example with which to evaluate the hydrodynamic forces in curved boundaries. The equilibrium distribution functions are set to all the fluid nodes. The hydrodynamic forces and the directions on the arc from outside of the arc are shown in Fig. 6 for both the methods. The insets in Figs. 6(a) and (b) show the errors from the evaluation from the exact solution. The method based on stress integration gives much smaller errors than that of the momentum exchange.

C. Sedimentation of a circular cylinder in a vertical channel

A circular cylinder moving in a channel under gravitational force has been extensively studied by Joseph *et al.* using a finite-element method [20–22]. In a previous paper [32], we used the momentum-exchange method to evaluate the hydrodynamic force on the circular particle. Excellent agreements between the lattice Boltzmann method and the second-order finite-element method by Joseph *et al.* [20–22] on the moving particles are obtained for the particle velocities in the vertical direction, the particle angular velocities, the forces in vertical direction, and torques at small Reynolds numbers, while there are small discrepancies between those two methods on the particle velocities and the forces in the horizontal direction. In the present paper we study the same flow problem using the lattice Boltzmann method with the stress-integration method.

The flow geometry is shown in Fig. 7 with the channel width $L=4d$, where $d=0.1$ cm is the diameter of the cylinder. The cylinder is released at $x=0.076$ cm and then settles under gravity. The density and the kinematic viscosity ν of the fluid are 1 g/cm^3 and 0.01 cm^2/s, respectively. In our simulation, the inlet of the domain is always $15d$ from the

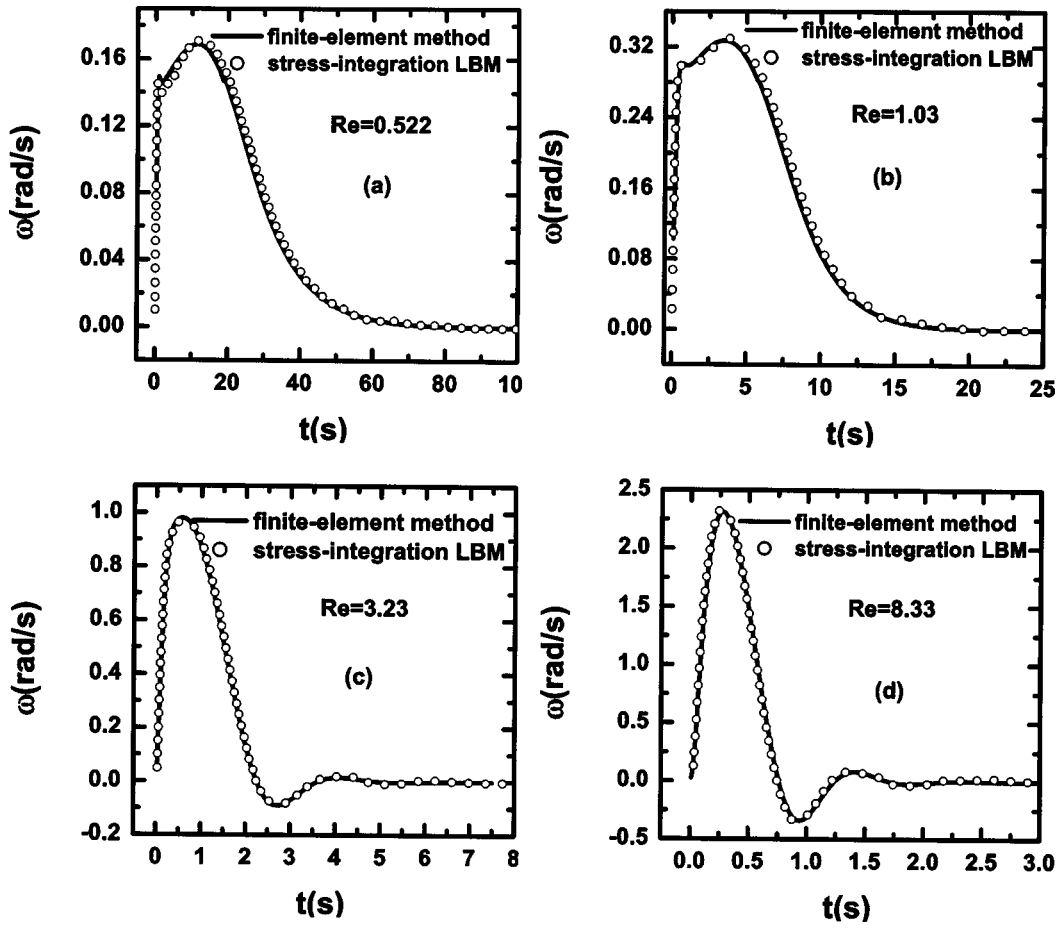

FIG. 11. The time-dependent angular velocity at different Reynolds numbers.

moving particles, whereas the downstream boundary is 15*d* or more from the boundary. Zero velocities are applied uniformly for the inlet and the normal derivative of the velocity is set to zero at outlet. The nonslip velocity condition is applied to the left and right solid walls. A periodic boundary condition is used for the top and bottom boundaries.

In the present lattice Boltzmann simulation, the radius of the cylinder is 13 lattice units. $\tau=0.6$. The translation of the center of the mass of a particle is updated at each Newtonian dynamics time step by using a so-called half-step "leap-frog" scheme [33]. The scheme is written as

$$\mathbf{V}\left(t+\frac{1}{2}\delta t\right)=\mathbf{V}\left(t-\frac{1}{2}\delta t\right)+\delta t\mathbf{F}_T(t)/M, \tag{21}$$

$$\mathbf{R}(t+\delta t)=\mathbf{R}(t)+\delta t\mathbf{V}\left(t-\frac{1}{2}\right)+\delta t^2\mathbf{F}_T(t)/M, \tag{22}$$

where $\mathbf{V}$ is the velocity of the center of mass of the solid particle, and M is the mass of the solid particle. For a two-dimensional system, the rotations of the particles are updated in a similar way. It should be noted that both local mass and momentum are conserved approximately on the boundaries as that discussed in detail in Ref. [30] although a point-wise interpolation scheme usually does not obey exact local mass and momentum conservation. We also note that the application of the volumetric representation [34] may improve the technique on the mass and momentum conservation.

Four cases with different solid fluid density ratios are simulated. In Fig. 8 the settling trajectories at different terminal Reynolds numbers from the lattice Boltzmann simulation with stress-integration method are shown together with the simulation results by a second-order finite-element method [21]. Excellent agreement between these two methods can be clearly seen. The terminal particle Reynolds number in the figure is defined by $Re=du_p/\nu$, where u_p is the terminal velocity of the particle. Figures 9–11 further display the time-dependent velocity and angular velocity at different terminal Reynolds numbers. The lattice Boltzmann simulation results agree with the finite-element simulation results to high accuracy.

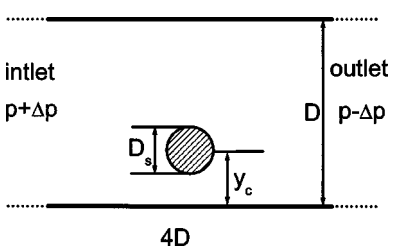

FIG. 12. A neutrally buoyant circular cylinder floating in Poiseuille flow.

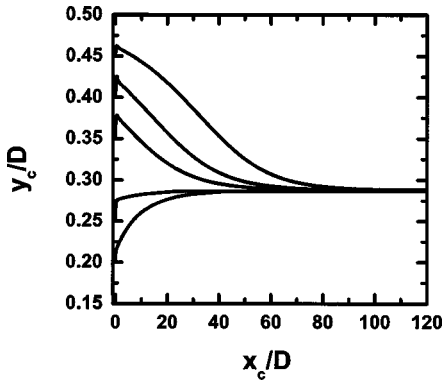

FIG. 13. Lateral migration from different initial positions of a cylinder a Poiseuille flow at Reynolds number Re=9.288 and for $D_s/D=0.25$,obtained by lattice Boltzmann simulations simulated with stress-integration method.

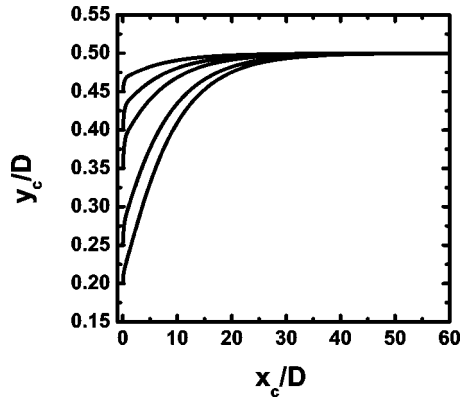

FIG. 14. Lateral migration from different initial positions of a cylinder in a Poiseuille flow for $D_s/D=0.25$, obtained by lattice Boltzmann simulations with the momentum-exchange method.

D. Motion of a neutrally buoyant circular cylinder in a Poiseuille flow

Segré and Silberberg [23] discovered that neutrally buoyant particles in a pipe flow will migrate laterally away both from the wall and the center line and reach a certain equilibrium lateral position. Karnis *et al.* [35] verified that this phenomenon is due to an inertia effect of the flow. Tachibana [36] found experimentally that when the ratio of the particle diameter to the pipe diameter exceeds 0.2, the phenomenon is more clear. Recently, Inamuro *et al.* [19] calculated the force and torque on the solid particle by integrating stress tensor and momentum flux on a closed surface for a fixed radial distance $0.16D$ from the surface of the cylinder, where D is the diameter of the cylinder. The Segré-Silberberg effect was observed in the simulation of a line of cylinders in a Poiseuille flow.

Figure 12 displays a schematic diagram in our lattice Boltzmann simulations of a single cylinder in a Poiseuille flow. The width of the tunnel is D while the diameter of the particle is D_s. The pressure drop from inlet to outlet is $2\Delta p$. In the simulations, the density of particles is $\rho_s=1$, while those of the fluid at inlet and outlet are $\rho_s \pm 3\Delta p$. $\tau=0.75$, $2\Delta p=0.00\,267$, Re=9.288, $D=100$, $D_s=25$, and $D_s/D=0.25$. The inlet and the downstream boundary of the domain are always $2d$ from the the moving particles. Pressure boundary conditions [37] are applied at the inlet and outlet. Initially, the particle is set at rest and let the fluid flow develop and approach steady state. At $t=10\,000$ time steps, the particle is released and will go from left to right.

The lateral migration curves of the cylinders released at different initial positions between the center line and the lower walls are shown in Figs. 13 and 14. It is found from Fig. 13 that the cylinders migrate to the same equilibrium position at $y_c/D=0.2874$ with the stress-integration method, which is a little closer to the center line than the lower wall. This value is a little larger than that in Ref. [19], which is 0.2733. The difference between our simulation and that in Ref. [19] is that we used the pressure boundary at the inlet and outlet while Inamuro *et al.* used a periodic boundary condition at the inlet and outlet so that they simulated a line of cylinders rather than a cylinder in a Poiseuille flow. On the other hand, the cylinder always migrates to the center line by using the method of momentum exchange, see Fig. 14.

VI. CONCLUSION AND DISCUSSION

The stress-integration method is used to evaluate the hydrodynamic force on an inclined plate, arc, and simulations of a circular cylinder settling in a vertical tube and in a Poiseuille flow. From the computations, the following results are obtained:

(1) In the calculations of the hydrodynamic force on an inclined boundary, the stress-integration method gives accurate results regardless of the length of the inclined boundary when there is no fluid flow. There are considerable errors when the method based on momentum transformation is applied. The stress-integration method is perhaps superior to the momentum-exchange method when there are elastic boundaries, on which the forces on small segments of boundaries have to be evaluated accurately to determine the motion of these small segments.

(2) The momentum-exchange method gives larger fluctuation in the calculation on the hydrodynamic forces on an arc, as shown in Fig. 5. The fluctuation becomes very small when the arc is closed as a full circle so that the momentum-exchange method works quite well in the calculation of the force on a resting circular cylinder.

(3) By simulating the sedimentation of a circular cylinder in a two-dimensional channel, excellent agreements between the current lattice Boltzmann method with the stress-integration method and a second-order finite-element method are obtained for the results of the time-dependent particle motions at small Reynolds numbers, including the particle velocities, the particle angular velocities, and the forces and torques on the moving particles.

(4) A particle migrated from the center line is found to occur in the simulations of a circular cylinder in a Poiseuille flow by the stress-integration method, consistent with the Segré-Silberberg effect.

Although the method based on stress integration uses extrapolation, which is more noisy and unstable, the method to calculate the stress tensor proposed by Inamuro *et al.* [19],

which avoids the calculation of the derivation of the velocity, and the choice of the rèlevant directions for extrapolation and enough points in the integration of the stress tensor in a lattice unit reduces the noise effectively. We emphasized that the formula to calculate the stress tensor [19] not only reduces the noise and instability of the lattice Boltzmann scheme, but also makes the code much simpler. The present conclusion should be useful for further development of lattice Boltzmann schemes with complex and moving boundaries, especially on the numerical simulations for blood flow [13,30,31,38].

ACKNOWLEDGMENTS

The authors thank Professor H. Hu for providing the data. This work was supported by the 100 Person Project of the Chinese Academy of Sciences and National Science Foundation of China under Grant Nos. 19834070 and 19904004.

[1] A. J. C. Ladd, J. Fluid Mech. **271**, 285 (1994).
[2] G. R. McNamara and G. Zanetti, Phys. Rev. Lett. **61**, 2332 (1988).
[3] Y. H. Qian, D. d'Humiéres, and P. Lallemand, Europhys. Lett. **17**, 479 (1992).
[4] S. Chen, H. Chen, D. O. Martinez, and W. H. Matthaeus, Phys. Rev. Lett. **67**, 3776 (1991).
[5] H. Chen, S. Chen, and W. H. Matthaeus, Phys. Rev. A **45**, 5339 (1992).
[6] A. J. C. Ladd, Phys. Rev. Lett. **76**, 1392 (1996).
[7] A. J. C. Ladd and R. Verberg, J. Stat. Phys. **104**, 1191 (2001).
[8] C. K. Aidun and Y. Lu, J. Stat. Phys. **81**, 49 (1995).
[9] C. K. Aidun, Y. Lu, and E. Ding, J. Fluid Mech. **373**, 287 (1998).
[10] D. Qi, J. Fluid Mech. **385**, 41 (1999).
[11] O. Behrend, Phys. Rev. E **52**, 1164 (1995).
[12] P. Raiskinmaki *et al.*, Comput. Phys. Commun. **129**, 185 (2000).
[13] C. Migliorini *et al.*, Biophys. J. **83**, 1834 (2002).
[14] R. Mei, D. Yu, W. Shyy, and L. Lou, Phys. Rev. E **65**, 041203 (2002).
[15] Z. G. Feng and E. E. Michaelides, Int. J. Multiphase Flow **28**, 479 (2002).
[16] K. Sankaranarayanan *et al.*, J. Fluid Mech. **452**, 61 (2002).
[17] D. S. Clague and P. J. Cornelius, Int. J. Numer. Methods Fluids **35**, 55 (2001).
[18] X. He and G. Doolen, J. Comput. Phys. **134**, 306 (1997).
[19] T. Inamuro, K. Maeba, and F. Ogino, Int. J. Multiphase Flow **26**, 1981 (2000).
[20] J. Feng, H. H. Hu, and D. D. Joseph, J. Fluid Mech. **261**, 95 (1994).
[21] H. H. Hu, D. D. Joseph, and M. J. Crochet, Theor. Comput. Fluid Dyn. **3**, 285 (1992).
[22] J. Feng, H. H. Hu, and D. D. Joseph, J. Fluid Mech. **277**, 271 (1994).
[23] G. Segré and A. Silberberg, Nature (London) **189**, 219 (1961).
[24] P. L. Bhatnagar, E. P. Gross, and M. Krook, Phys. Rev. A **94**, 511 (1954).
[25] X. He and L-S. Luo, Phys. Rev. E **56**, 6811 (1997).
[26] T. Abe, J. Comput. Phys. **131**, 241 (1997).
[27] O. Filippova and D. Hanel, Comput. Fluids **26**, 697 (1997).
[28] R. Mei, L. Lou, and W. Shyy, J. Comput. Phys. **155**, 307 (1999).
[29] H. P. Fang, Z. F. Lin, and Z. W. Wang, Phys. Rev. E **57**, R25 (1998).
[30] H. P. Fang, Z. W. Wang, Z. F. Lin, and M. R. Liu, Phys. Rev. E **65**, 051925 (2002).
[31] A. G. Hoekstra *et al.*, Lect. Notes Comput. Sci. **2657**, 997 (2003).
[32] H. P. Fang, D. R. Noble, H. H. Hu, and S. Y. Chen, J. Comput. Phys., to be published.
[33] M. P. Allen and D. J. Tildesley, *Computer Simulation of Liquid* (Clarendon, Oxford, 1987).
[34] H. D. Chen, Phys. Rev. E **58**, 3955 (1998).
[35] A. Karnis, H. L. Goldsmith, and S. G. Mason, Can. J. Chem. Eng. **44**, 181 (1966).
[36] M. Tachibana, Rheol. Acta **12**, 58 (1972).
[37] Q. Zou and X. He, Phys. Fluids **9**, 1591 (1997).
[38] M. Hirabayashi *et al.*, Phys. Rev. E **68**, 021918 (2003).